Journal of Optoelectronics and Advanced Materials Vol. 3, No. 2, June 2001, p. 199 - 214

ATOMIC AND ELECTRONIC STRUCTURES OF GLASSY Ge_XSe_{1-X} AROUND THE STIFFNESS THRESHOLD COMPOSITION

S. Hosokawa

Institut für Physikalische-, Kern-, und Makromolekulare Chemie, Philipps Universität Marburg, D-35032 Marburg, Germany

Anomalous x-ray scattering experiments on glassy Ge_xSe_{1-x} have been carried out at energies close to the Ge and Se K edges at concentrations close to the onset and completion of the rigidity percolation threshold (x = 0.195 and 0.23). The total structure factors $S(Q)$ show rapid changes in both the position and intensity of the prepeak around 10 nm^{-1}, while remaining almost unchanged in the other Q ranges. The differential structure factors $\Delta_i S(Q)$ obtained have characteristic features of their own. A detailed comparison among them suggests that the prepeak originates from only the Ge-Ge correlation. On the basis of the concentration dependence of the spectra and the existing partial structure factors of glassy $GeSe_2$ obtained by Petri *et al.*, the origin of the prepeak is discussed. Valence- and conduction-band electronic density of states of glassy Ge_xSe_{1-x} ($0 \leq x \leq 0.33$) were also investigated by measuring the ultraviolet photoemission and inverse-photoemission spectra. They exhibit a remarkable change in their spectral features near x = 0.20. These observations in both the atomic and electronic structures are consistent with the occurrence of a percolation threshold in non-crystalline covalent network systems as predicted by Phillips and Thorpe. The threshold is characterized by the percolation of a specific $Ge(Se_{1/2})_4$ molecular unit spread over the network.

(Received May 28, 2001; accepted June 11, 2001)

Keywords: Electronic structure, Stiffness threshold, Ge_XSe_{1-X} glass

1. Introduction

There is a general agreement that in glassy (g-) Ge_xSe_{1-x} systems, the coordination numbers of Ge and Se are 4 and 2, respectively, in the concentration range $0.00 \leq x \leq 0.33$. This chemically-ordered continuous-random-network model was originally proposed by Zachariasen [1], and experimentally supported by electron diffraction- [2,3], x-ray diffraction- [4], and Raman scattering [5] measurements.

Mean-field constraint theory [6,7] for network glasses provides a powerful tool to explain the experimentally observed numerous anomalies around the critical composition of rigidity percolation threshold at an average coordination number, $\langle r \rangle = 2.4$, where the number of constraints per atom is equal to the degree of freedom. In case of g-Ge_xSe_{1-x} systems, this corresponds to x = 0.20. The character of the network glass undergoes a steep "first-order-like" transition from easily deformable at $\langle r \rangle < 2.4$ (*floppy*) to *rigid* at $\langle r \rangle > 2.4$. Katamigahara *et al.* [8] reported a dynamic density of states around 5 meV to prove the existence of the *floppy* mode (*zero-frequency* mode in the *floppy* glass) by measuring inelastic neutron scattering spectra. Recently, Boolchand and co-workers [9] demonstrated that results from Raman scattering, modulated scanning calorimetry, molar volume, and Mössbauer spectroscopy provide evidence for a multiplicity of stiffness transitions; an onset point near $\langle r \rangle = 2.40$ (x = 0.20) and a completion point near $\langle r \rangle = 2.46$ (x = 0.23). Of particular interest are the Raman scattering results of the concentration variation of corner-sharing mode frequency of $Ge(Se_{1/2})_4$ units, which show an abrupt jump at x = 0.23. These Raman results led to the suggestion that they correlate rather well with the atomic and electronic structures of g-Ge_xSe_{1-x} around this stiffness threshold composition.

X-ray absorption fine structure (XAFS) results provide excellent information on first-shell local structure, or the so-called short-range order (SRO), around each constituent element even in non-crystalline materials. For this reason, precise studies of the concentration dependence of the atomic structure of g-Ge_xSe_{1-x} in the range $0.00 \leq x \leq 0.33$ were performed using XAFS technique

[10,11,12]. They confirmed the predicted coordination numbers (8–*N* rule) with the bond length similar to that in the crystal. Only ref. [12] suggests minor deviations of the coordination numbers from the 8–*N* rule. The higher shell information was, however, very limited due to a short lifetime of photoexcited electrons during the XAFS process.

An x-ray diffraction study was performed at compositions x = 0.00, 0.04, 0.10, 0.15, 0.20, and 0.25 [13], which demonstrated that besides the well-established SRO information, a prepeak appears in the total structure factors $S(Q)$ at a scattering vector Q of about 10 nm^{-1}. The prepeak, which is clear evidence for the existence of intermediate-range order (IRO), shows a systematic decrease in the intensity and shifts towards higher Q with decreasing Ge concentration. The earlier x-ray scattering experiment [4], as well as a recent neutron diffraction measurement [14], indicated the same concentration variation of the prepeak in $S(Q)$.

An anomalous x-ray scattering (AXS) experiment was carried out by Armand *et al.* [15] at x = 0.167 and 0.25. From the differential structure factors $\Delta_i S(Q)$ obtained, they concluded that the structure at x = 0.25 is based on that of the crystalline $GeSe_2$ with the presence of edge- and corner-sharing $Ge(Se_{1/2})_4$ tetrahedra, and that at x = 0.167, the structure is built up from isolated $Ge(Se_{1/2})_4$ tetrahedra interconnected by short Se chains. Moreover, they suggested that the prepeak seems to be due to the Ge-Ge correlations. However, due to the rough concentration steps at which the diffraction experiments were performed, it is still difficult to discuss how the IRO in g-Ge_xSe_{1-x} changes when crossing the stiffness threshold composition x = 0.20.

We have carried out AXS experiments on g-Ge_xSe_{1-x} [16] to obtain detailed structural information, *i.e.*, to clarify the role of each element on the SRO and IRO. The experiments were performed at the Ge concentrations of 0.195 and 0.23, which are respectively very close to the onset and completion concentration points of the Boolchand's criterion [9]. Additionally an $S(Q)$ measurement was performed at x = 0.185.

As mentioned above, the Raman scattering results of the corner-sharing mode frequency of $Ge(Se_{1/2})_4$ units show a sudden jump at x = 0.23 [9]. The origin of the covalent bond is, of course, a distribution of electron clouds between atoms. Valence-band electronic density of states can be investigated by means of photoemission spectroscopy (PES). Some decades ago, PES spectra of g-$GeSe_2$ [17,18,19] and g-Se [20] were obtained using this technique. The results confirmed simple band models for each glass.

On the other hand, information on the conduction bands or the empty states has been limited so far. Measurements of optical reflectance [19,21,22] is one of the indirect methods to estimate the conduction bands. The imaginary part of dielectric function, ε_2, can be calculated by a Kramers-Kronig analysis of the reflectance spectra. The ε_2 spectrum was for a long time believed to be the simple convolution of the valence and conduction bands, which is the so-called constant-transition-matrix-element assumption for disordered materials. However, our recent PES-IPES works on g-Se and As_2Se_3 [23] and amorphous Ge [24] provide the first clear-cut evidence that this historic assumption is not generally valid. Core-absorption spectroscopy [18,25,26,27] was also widely used to obtain information on the empty states. However, it was very difficult to obtain the conduction-band DOS from the reflectance and core-absorption measurements, because the role of the exciton effects as well as the matrix elements on these optical transitions were not sufficiently understood for analysing them further.

It is well known that inverse-photoemission spectroscopy (IPES) is a powerful method to directly obtain conduction-band DOS. We have measured PES and IPES spectra of g-Ge_xSe_{1-x} in the concentration range $0 \leq x \leq 0.33$, especially near x = 0.20 in detail, and found a dramatic change in the spectral features near x = 0.20 [28].

In this paper, I review our recent investigations on the atomic and electronic structures of g-Ge_xSe_{1-x} near the stiffness threshold composition x = 0.20 by means of the AXS and PES/IPES measurements. Following this section, principles of these noble techniques and actual experimental procedures are given in Sec. II and III, respectively, with separated subsections for each technique. Then, the experimental results are presented in Sec. IV. In Sec. V, I discuss the critical behaviours of the atomic and electronic structures in g-Ge_xSe_{1-x} mixtures in terms of the Phillips-Thorpe rigidity percolation theory [6,7]. I conclude in the last section.

2. Principles of experimental techniques

A. Anomalous x-ray scattering

The scattered x-ray intensity varies with energy E of the incident x-ray beam due to the energy dependence of the atomic form factor,

$$f(Q,E) = f_0(Q) + f'(E) + if''(E), \tag{1}$$

where f_0 is the energy-independent form factor, f' and f" the real and imaginary parts of anomalous term, respectively. When the incident x-ray energy is tuned near an absorption edge of an element in a multicomponent material, the variation of $f(Q,E)$ is significant, which can produce a substantial contrast among the scattering patterns, *i.e.*, $S(Q)$, recorded at different energies. As an example, f' and f" of Ge and Se are shown in Fig. 1 as a function of energy E, which were calculated by Sasaki [29]. As is clearly seen in the figure, each f' exhibits a considerable decrease at energies near its K absorption edge.

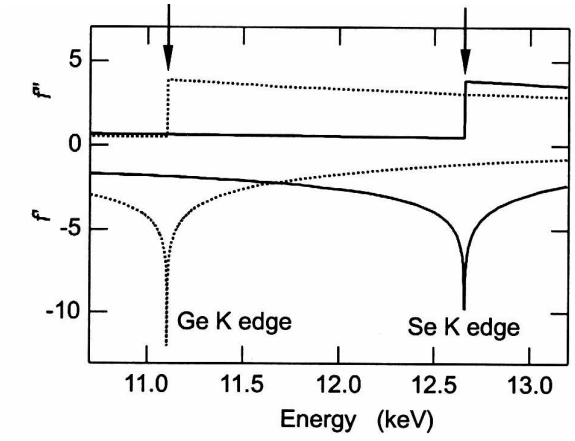

Fig. 1. f' and f" of Ge (dashed lines) and Se (solid lines) as a function of energy E calculated by Sasaki [29]. Arrows indicate energies at K absorption edges.

This contrast can be used to obtain $\Delta_i S(Q)$ by taking the difference of two scattering spectra measured typically at about 10 eV and some hundred eV below the absorption edge. The $\Delta_i S(Q)$ mainly results from pair correlations of the element near whose absorption edge the experiments are carried out. For example, for a binary alloy AB, if the measurements are performed close to an absorption edge of A element, the $\Delta_A S(Q)$ usually contains only A-A and A-B correlations, because $f(Q,E)$ of B element does not change significantly over the energy range used, and thus the B-B correlation is eliminated by taking the difference. Like XAFS, AXS provides selective information on the structural environment around a specific element. A distinct advantage of AXS compared to XAFS is that it provides a sensitive IRO information as already mentioned in the introductory section.

The pair distribution function $g(r)$ of an average atom is expressed as

$$4\pi r\rho_0\left[g(r)-1\right] = \frac{2}{\pi}\int Q\left[S(Q)-1\right]\sin Qr\,dQ \tag{2}$$

where ρ_0 is the averaged number density. $S(Q)$ is related to the elastically scattered x-ray intensity $I(Q,E)$ by

$$\alpha I(Q,E) = \left\langle f(Q,E)^2 \right\rangle - \left\langle f(Q,E) \right\rangle^2 + \left\langle f(Q,E) \right\rangle^2 S(Q) \tag{3}$$

where α is a normalization constant, and <> represents the chemical average of the atomic form factors, *i.e.*, for a binary alloy,

$$\left\langle f(Q,E)^2 \right\rangle = \sum_{i=1}^{2} c_i \left| f_i(Q,E) \right|^2 \tag{4}$$

and

$$\left\langle f(Q,E) \right\rangle^2 = \left[\sum_{i=1}^{2} c_i f_i(Q,E) \right]^2. \tag{5}$$

Here c_i is the atomic fraction of element i. Then, $S(Q)$ can be written as a linear combination of three partial structure factors, $S_{ij}(Q)$, weighted by weighting factors $W_{ij}(Q,E)$,

$$S(Q,E) = \sum_{i=1}^{2} \sum_{j=1}^{2} W_{ij}(Q,E) S_{ij}(Q), \tag{6}$$

where

$$W_{ij}(Q,E) = c_i c_j \frac{f_i(Q,E) f_j(Q,E)}{\left\langle f(Q,E) \right\rangle^2}, \tag{7}$$

The imaginary part of anomalous terms $f''(E)$ in the atomic form factors can be experimentally obtained from XAFS experiments, and $f'(E)$ can be calculated from $f''(E)$ using the Krammers-Kronig relation [30,31,32]. However, the difference between the theory and their experimental results are small in the energy range more than 15 eV below the absorption edge. Therefore, theoretical data calculated by Sasaki [29] were used for the present analyses. Theoretical value of the energy-independent form factor f_0 was also taken from a literature [33]. The energies and corresponding theoretical values of $f'(E)$ and $f''(E)$ used for our experiments and analyses are given in Table 1.

Table 1. f' and f'' values (electron units) of Ge and Se elements at energies measured.

Energy (eV)	f'_{Ge}	f''_{Ge}	f'_{Se}	f''_{Se}
10903	–3.647	0.510	–1.750	0.656
11088	–6.292	0.494	–1.844	0.635
12454	–1.254	3.157	–3.725	0.515
12639	–1.113	3.084	–6.141	0.500

Fig. 2(a) shows the weighting factors W_{ij} of Ge-Ge, Ge-Se, and Se-Se atomic correlations for g-$Ge_{0.23}Se_{0.77}$ at the incident energy of 10903 eV (–200 eV from the Ge K edge) as a function of Q. Due to the dominant concentration of Se in g-$Ge_{0.23}Se_{0.77}$, the largest contribution is W_{SeSe} of about 65%, the second W_{GeSe} of about 30%, and the smallest W_{GeGe} of about 5%. They slightly change with Q.

As mentioned above, for analysing the local structures, one can use the difference of the scattering intensities,

$$\Delta I(Q) = \Delta\left[\left\langle f^2 \right\rangle - \left\langle f \right\rangle^2\right] + \Delta\left[\left\langle f \right\rangle^2\right] \Delta S(Q), \tag{8}$$

where Δ indicates the difference between energies E_1 and E_2 of the following quantity. If the energies are chosen so that mainly i element's $f(Q,E)$ changes, *i.e.*, E_1 is relatively far (some hundred eV) from the i element's absorption edge, and E_2 very close (about 10 eV) to it, Eq. (8) is very sensitive to correlations comprising i element. $\Delta S(Q)$ is also defined as a linear combination of $S_{ij}(Q)$,

$$\Delta S(Q) = \sum_{i=1}^{2} \sum_{j=1}^{2} W_{ij}(Q,E_1,E_2) S_{ij}(Q), \tag{9}$$

where the weighting factors are

$$W_{ij}(Q,E_1,E_2) = c_i c_j \frac{\Delta\left[f_i f_j\right]}{\Delta\left[\left\langle f \right\rangle^2\right]}. \tag{10}$$

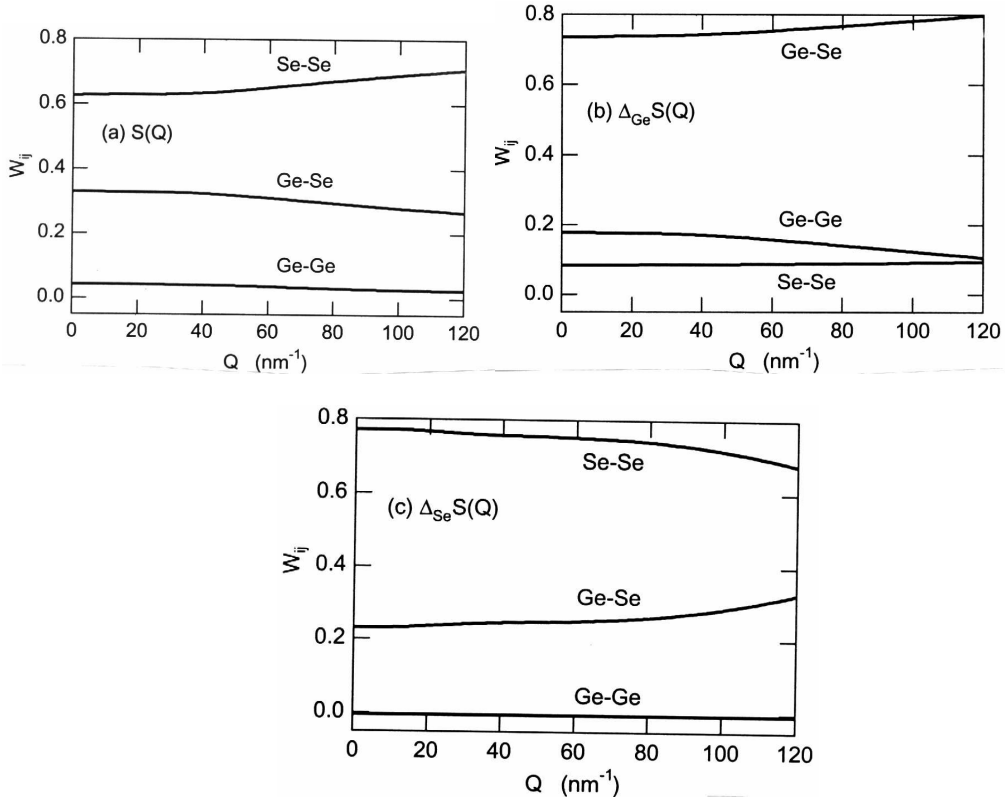

Fig. 2. W_{ij} of Ge-Ge, Ge-Se, and Se-Se atomic correlations in (a) $S(Q)$ for g-$Ge_{0.23}Se_{0.77}$ at the incident energy of 10903 eV (200 eV below the Ge K edge), in (b) $\Delta_{Ge}S(Q)$, and in (c) $\Delta_{Se}S(Q)$ as a function of Q.

For g-$Ge_{0.23}Se_{0.77}$, W_{ij}s obtained from two different energies close to the Ge and Se K edges, *i.e.*, those in $\Delta_{Ge}S(Q)$ and $\Delta_{Se}S(Q)$, in the present experiments are shown in Figs. 2(b) and 2(c), respectively. As seen in Fig. 2(b), the Se-Se correlation is highly suppressed in comparison to W_{SeSe} for $S(Q)$ shown in Fig. 2(a). However, the Ge-related weighting factors (Ge-Ge and Ge-Se) are considerably larger in $\Delta_{Ge}S(Q)$ than in $S(Q)$. On the other hand, the Ge-Ge correlation in $\Delta_{Se}S(Q)$ shown in Fig. 2(c) is negligibly small, whereas the Se-related correlations are highly enhanced. They slightly change with Q.

B. Photoemission and inverse-photoemission spectroscopies

Photoelectron or photoemission spectroscopy (PES) is well known as a technique to evaluate valence-band electron density of states (DOS) using the photoelectron effect. Fig. 3(a) shows a schematic band scheme to explain how one can obtain the occupied-state DOS by means of the PES measurement. When a light photon irradiates a material, an electron is excited with the corresponding energy of the photon, $h\nu$, when the final state is empty for excitation.

Inverse-photoemission spectroscopy (IPES) or Bremsstrahlung Isochromat spectroscopy (BIS) is a relatively new technique to investigate conduction-band DOS. The word ‘inverse-‘ means phenomenologically inverse to the PES procedure, but the process of the IPES is not inversely. Figure 3(b) shows a schematic band scheme to explain how one can obtain the conduction-band or empty-state DOS by means of IPES measurement. When a material is irradiated by an electron with a kinetic energy of E_K, the electron enters an empty (conduction-band) state of the material with the corresponding energy. This electron can radiatively loose its energy by releasing to a conduction-band state with a lower energy level, and emits a photon with the corresponding energy $h\nu$. Hence, one can estimate the conduction-band DOS by measuring the energy and intensity of the photons coming from the surface of material.

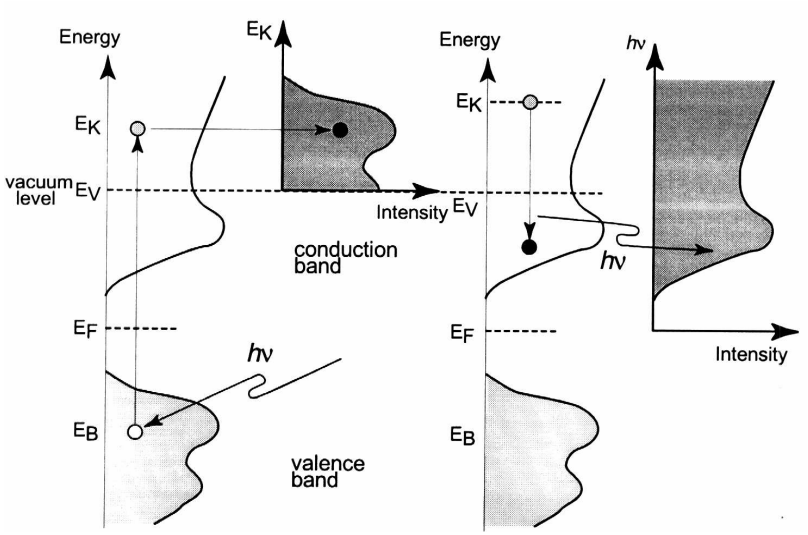

Fig. 3. Schematic band scheme to explain how one can obtain (a) valence-band and (b) conduction - band DOSs by means of the PES and IPES measurements, respectively.

Technically, the PES and IPES measurements must be performed under ultrahigh vacuum conditions of better than 10^{-9}-10^{-10} Torr (or mbar). This is because the PES and IPES processes occur near the surface of material (1-10 nm) and a contamination by oxygen *etc.* causes fatal effects to the PES and IPES spectra. The sample surface must be clean on the atomic level. Additionally, if the sample is not metallic, such as the present semiconducting Ge-Se system, an electrostatic charging of the sample must carefully be avoided in the IPES process. The injected electron can smoothly be escaped from the sample surface to the ground by preparing the nonmetallic sample with a thickness of 1-10 nm.

3. Experimental procedure

A. Anomalous x-ray scattering

The Ge_xSe_{1-x} bulk samples were prepared by quenching the melts after rocking the quartz ampoule of the mixed compound for at least 48 hours. The purity of each starting element was 99.999%. The concentration and homogeneity of the samples were examined by measuring Raman scattering spectra at several parts of the quenched samples.

The AXS measurements were carried out using an ω–2θ diffractometer installed at the beamline BM02 of the European Synchrotron Radiation Facility (ESRF) in Grenoble, France. X-rays produced by a bending magnet were monochromatized using an Si(111) double-crystal monochromator with a sagittal focusing shape, which was located between two cylindrically bent mirrors. This x-ray optics provided a small size of incident x-ray beam with 0.2 mm height and 0.5 mm width, and an energy resolution of about 1 eV. Energy was calibrated using the L_{III} absorption edge of an Au foil (11918 eV) before the experiments, and additionally *in situ* by using the Ge and Se K edges of the sample during the experiments.

The diffraction experiments were performed at two energies (–15 and –200 eV) below the K edge of each element (Ge: 11103 eV, Se: 12654 eV). In order to obtain $\Delta_i S(Q)$s, or partial structure factors $S_{ij}(Q)$, of good statistical quality, there are two requirements which need to be fulfilled: 1) A sufficient energy resolution of the detector to discriminate the elastic signal from the fluorescence and Compton contributions, and 2) a sufficient number of scattered x-ray photons in a reasonable data acquisition time. In case of the present samples near $Ge_{0.2}Se0_{0.8}$ concentration, provided that 30,000 counts at the Q position of the first $S(Q)$ maximum give enough statistical quality, 600,000 counts at the same Q position are necessary to obtain $\Delta_{Ge}S(Q)$ of identical quality. This is because the contrast in the vicinity of the Ge K absorption edge is only about 5%. At least three times more counts would even be needed to obtain $S_{ij}(Q)$s. For these reasons, we chose a pyro-graphite crystal analyzer, which

provides a good Bragg reflection efficiency. The scattered x-ray photons were energy-analysed with this crystal, and counted using a photomultiplier with NaI crystal scintillators. To satisfy the first requirement mentioned above, the detector was placed on a long arm of 40 cm.

Fig. 4 shows rocking curves obtained from this detector system measured close to the Se K edge (–15 and –200 eV) at Q = 60 nm^{-1}, where the nonelastic contributions to the elastic signal are large. The energy resolution of this detector system was about 90 eV in these energy ranges. The dotted curves are ten times enlarged in comparison to the solid curves to clearly show the Se K_β fluorescence and Compton scattering intensities. As seen in the figure, both the Se K_β and Compton contributions can be estimated to be less than 0.3% at energies where the elastic spectra were measured (arrows in Fig. 4). Nevertheless, we measured such rocking curves for each scan at Q = 12, 22, 40, 60, and 90 nm^{-1} to estimate these contributions in order to use them for the data correction. Similar rocking curves were also obtained close to the Ge K absorption edge.

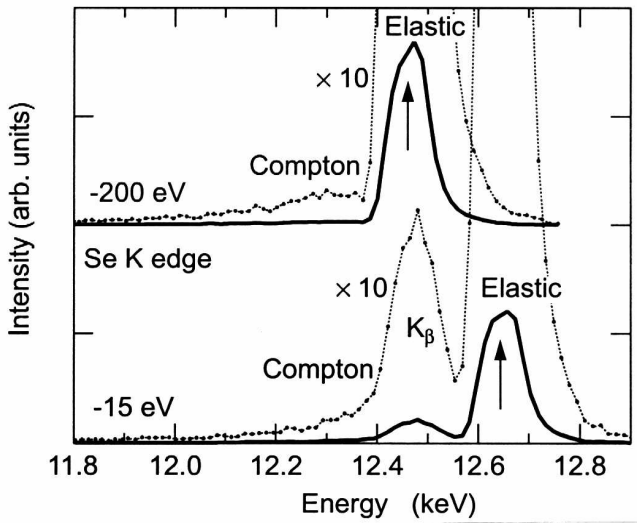

Fig. 4. Rocking curves of the detector system measured at energies close to the Se K absorption edge at Q = 60 nm^{-1}.

The diffraction measurements were performed in steps of 0.5 nm^{-1} in the Q range from 4 nm^{-1} up to 94 and 109 nm^{-1} at energies close to the Ge and Se K edges, respectively. More than 600,000 counts at the Q position of the first $S(Q)$ maximum could be acquired at the incident energies close to the Ge edge, and 180,000-250,000 counts close to the Se K edge. The data collection durations were about 4 and 6 hours for each scan around the Ge and Se K edges, respectively. The incident beam intensity was monitored by counting the scattering signal from a thin Kapton foil in front of the sample using a photomultiplier with NaI crystal scintillators, and used for the normalization of the spectra.

B. Ultraviolet photoemission and inverse-photoemission spectroscopies

Fig. 5 shows a schematic diagram of the experimental apparatus used for recording the ultraviolet PES (UPS) and IPES spectra. It is mainly composed of four ultrahigh-vacuum chambers: two chambers for the sample preparation, an IPES analyser chamber and an UPS analyser chamber, operating under base pressures of 4.0×10^{-10}, 7.0×10^{-11}, and 4.0×10^{-10} Torr, respectively.

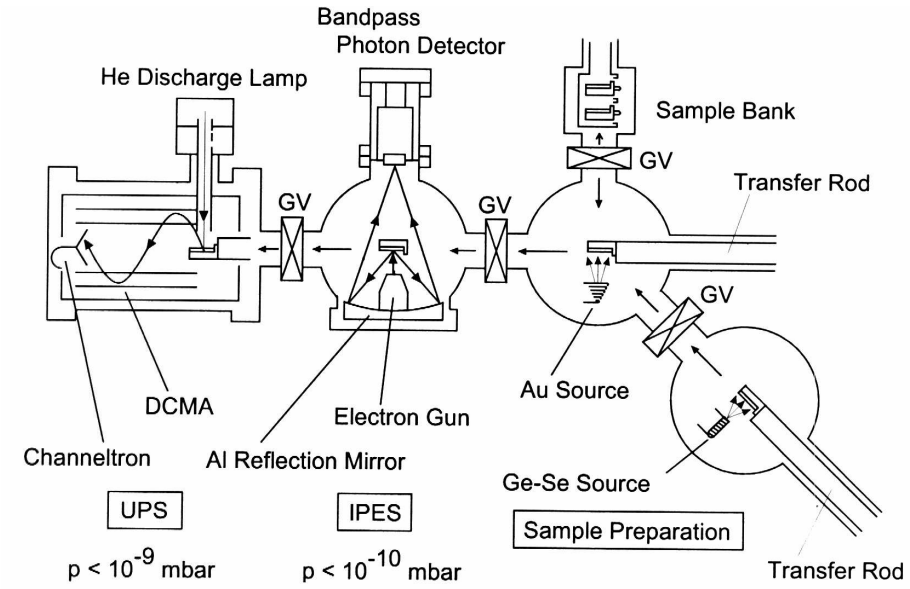

Fig. 5. Schematic diagram of the apparatus composed of the UPS and IPES spectrometers, and two sample preparation chambers. The *in situ* measurements of the UPS and IPES spectra enable us to connect the both spectra at the Fermi level.

In the IPES chamber, a monoenergic electron beam from an electron gun of Erdman-Zipf type with a BaO cathode, which can deliver a high beam current down to low kinetic energy (1-10 μA at 10 eV) with an energy spread of 0.25 eV, was focused onto the sample. Light emitted from the sample was focused by an Al reflection mirror coated with an MgF_2 film and detected using a bandpass photon detector of our own design [34]. The detector consists basically of a simple combination of a pure SrF_2 entrance window and a commercial Cu-BeO photomultiplier. Evaporation of KCl onto the first dynode of the photomultiplier improved the bandpass characteristics and the sensitivity. The full-width at half-maximum of the detector was 0.47 eV centred at 9.43 eV. The sensitivity was increased by about one order of magnitude in comparison to the original one. The overall energy resolution of the spectrometer was 0.56 eV [35].

The UPS spectrometer was composed of a He discharge lamp ($h\nu$ = 21.2 eV) as an excitation light and a double-stage cylindrical-mirror analyser (DCMA) as an electron energy analyser for recording angle-integrated spectra. The energy resolution of the UPS spectrometer was set to be 0.2 eV. The energy calibrations of the IPES and UPS spectra were experimentally performed using the spectra measured for the same surface of a fresh polycrystalline Au film, and the energy scale were connected at the Fermi level.

The source alloys for the sample preparation were prepared by a standard melt quenching method using mixed alloys from commercial samples of $GeSe_2$ and Se with purity of 99.999% each, in quartz ampoules. Each *g*-Ge_xSe_{1-x} film sample was prepared *in situ* by evaporating the source alloy onto a fresh Au film, which was evaporated onto a metal substrate. The Au film is inactive against the sample. The evaporation was performed in one of the preparation chambers using a quartz furnace under a vacuum of about 1.5×10^{-9} Torr during the evaporation. The composition of films with a thickness of ~3 μm was carefully determined by electron-probe microanalysis. They were in all cases close to the starting composition within 2-3%.

For the UPS an IPES measurements, the thickness of films was reduced to 5-10 nm to avoid an electrostatic charging effect in the IPES measurements as mentioned in Sec II(B). After the UPS and IPES measurements, the UPS spectra for these thin films were checked to be fully consistent with those of the thick films in order to determine the concentrations. The deposition rate was controlled by means of a quartz thickness monitor placed close to the sample substrate. The typical deposition rate was 20-30 pm/sec. We also checked carefully the contamination of the samples during the measurements by observing the change of the UPS spectra repeatedly, because the typical effect of the contaminants appears in the valence-band DOS.

4. Results

Fig. 6(a) and (b) show elastic scattering intensities $\alpha I(Q,E)$ for g-$Ge_{0.23}Se_{0.77}$ at energies close to the Ge and Se K edges, respectively, as a function of Q, together with $\langle f \rangle^2$. The intensities are normalized to the electron unit using the method proposed by Krogh-Moe [36] and Norman [37]. As clearly seen in the figures, distinct contrast appears with a small energy change of the incident x-rays around the absorption edges. Especially in Fig. 6(a), the intensity increases at the Q value of the first maximum around 20 nm^{-1} when the incident x-ray energy approaches to the Ge K edge, although $\langle f \rangle^2$ decreases. Such an anomaly is also seen in Fig. 6(b) at the prepeak position around 10 nm^{-1} when the energy approaches to the Se K edge. The same trend is also seen in g-$Ge_{0.195}Se_{0.805}$.

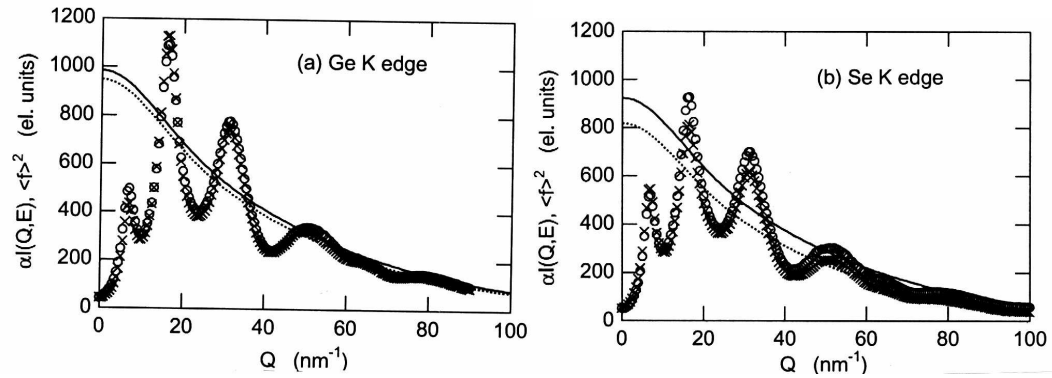

Fig. 6. Normalized elastic scattering intensities $\alpha I(Q,E)$ (marks) for g-$Ge_{0.23}Se_{0.77}$ at energies close to the (a) Ge and (b) Se K edges as a function of Q, together with $\langle f \rangle^2$ (lines). Circles and solid lines indicate the values at-200eV below the absorption edge, and crosses and dashed lines at-15eV.

The $S(Q)$ spectra can be calculated by using Eq. (3). Fig. 7(a) shows the concentration dependence of $S(Q)$ measured at the incident x-ray energy of 10903 eV (200eV below the Ge K edge) at x = 0.23 (crosses), 0.195 (triangles), and 0.185 (circles). For clarity, the spectra are shifted against one another by 0.2. In the large Q range beyond 40 nm^{-1}, they are extremely similer. On the other hand, the magnitudes of the first and second peaks at Q = 20.5 and 35.2 nm^{-1}, respectively, slightly decrease with decreasing x, while their Q positions remain unchanged. The prepeaks in the $S(Q)$s are shown in Fig. 7(b) on an enlarged scale, along with the previous results at x = 0.25 (dashed line) and 0.167 (solid line) [15]. It can be clearly seen in the figure that a decrease in the Ge concentration x leads to a rapid decrease of the intensity of prepeak, and its position considerably shifts to higher Q values.

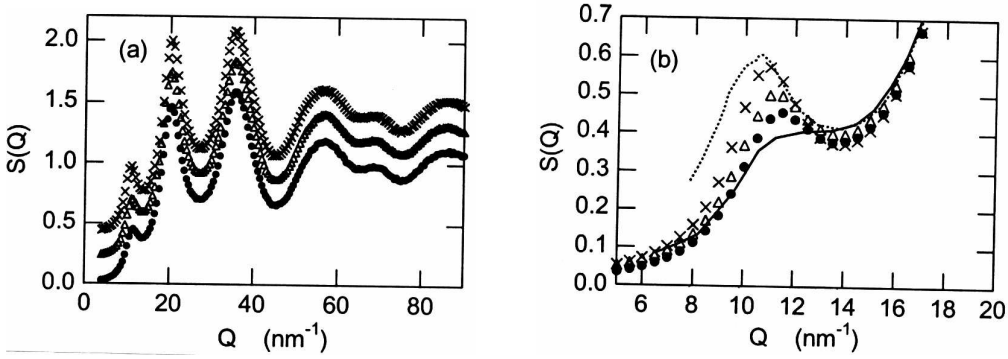

Fig. 7. (a) Concentration dependence of $S(Q)$ measured at E = 10903 eV (200 eV below the Ge K edge) and at x = 0.23 (crosses), 0.195 (triangles), and 0.185 (circles). For clarify, the spectra are shifted against one another by 0.2. (b) $S(Q)$s around the prepeak position on an enlarged scale, along with the previous results [15] at x = 0.25 (dashed line) and 0.167 (solid line).

Fig. 8 shows $\Delta_i S(Q)$s for g-$Ge_{0.195}Se_{0.805}$ close to the Ge (crosses) and Se (circles) K edges. For comparison, $S(Q)$ measured at 10903 eV is also displayed as a solid line. The shape of $\Delta_{Ge}S(Q)$ is very different from that of $S(Q)$, *i.e.*, it has a much larger prepeak at Q = 11 nm^{-1} in comparison to $S(Q)$. It

shows a large minimum with negative sign at the first peak position in $S(Q)$ at Q = 20.5 nm^{-1}. The second peak in $S(Q)$ at Q = 35.2 nm^{-1} disappears in $\Delta_{Ge}S(Q)$. On the other hand, $\Delta_{Se}S(Q)$ has almost no signal at the prepeak position, while it is very similar to $S(Q)$ beyond the Q position of the first peak (Q > 20 nm^{-1}). Closely similar results were obtained for g-$Ge_{0.23}Se_{0.77}$ as seen in Fig. 9.

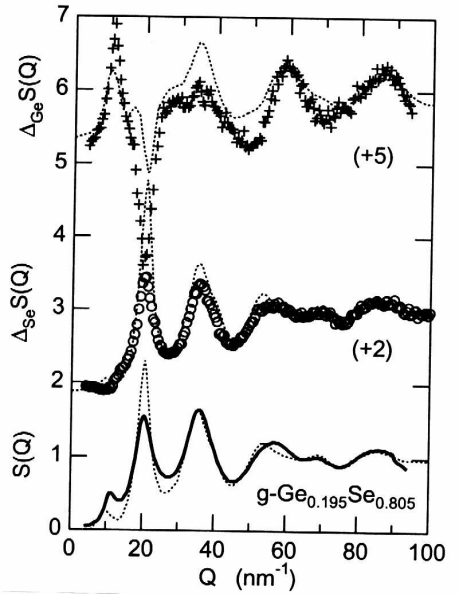

Fig. 8. $\Delta_i S(Q)$s for g-$Ge_{0.195}Se_{0.805}$ close to the Ge (crosses) and Se (circles) K edges together with $S(Q)$ (solid line) measured at E = 10903 eV (200 eV below the Ge K edge). Dotted lines indicate spectra calculated from $S_{ij}(Q)$s for g-$GeSe_2$ measured by Petri et al. [39]. See text for detail.

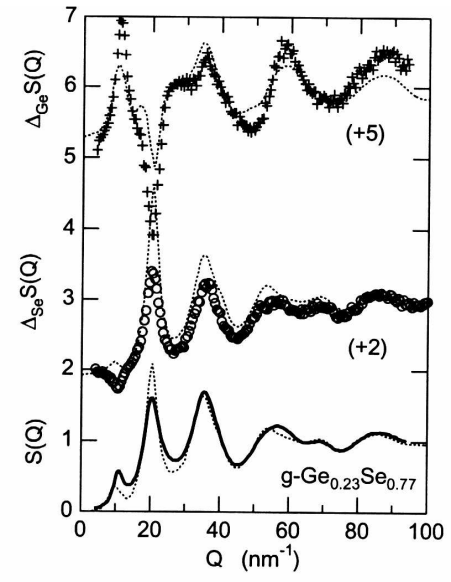

Fig. 9. $\Delta_i S(Q)$s and $S(Q)$ for g-$Ge_{0.23}Se_{0.77}$. Explanations are the same as in Fig. 8.

Fig. 10 shows a series of valence-band UPS and conduction-band IPES spectra on g-Ge_xSe_{1-x} with x from 0 to 0.33. Intensities of the UPS spectra are normalized at –2.7 eV, and those of the IPES spectra at 3.1 eV (x = 0, 0.10, 0.15, and 0.18) and 2.4 eV (x = 0.20, 0.25, and 0.33). Vertical bars indicate the positions of the peaks. Energies are referred to the Fermi level.

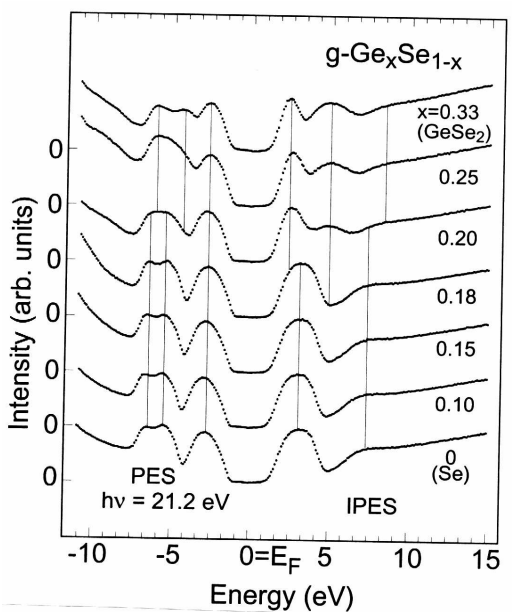

Fig. 10. A series of valence-band UPS and conduction-band IPES spectra on g-Ge_xSe_{1-x} with x from 0 to 0.33. Intensities of the UPS spectra are normalized at –2.7 eV, and those of the IPES spectra at 3.1 eV (x = 0, 0.10, 0.15, and 0.18) and 2.4 eV (x = 0.20, 0.25, and 0.33). Vertical bars indicate the positions of the peaks. Energies are referred to the Fermi level.

The UPS spectra for g-Se (x = 0) show distinct structures at –2.7, -5.4, and –6.4 eV, which are in good agreement with previous data [20] although in this case the samples were much thicker. The IPES spectra have also clear structures at 3.1 and 7.4 eV in good agreement with our previous measurements [23]. With increasing the Ge concentration from x = 0 to 0.18, the UPS and IPES spectra do not show any noticeable change in the spectral shape and the energy positions of peaks. With a further increase of the Ge concentration x by only 2%, however, the IPES spectra drastically change to another shape with mainly three peaks; a sharp peak at 2.4 eV, a relatively broad peak at 4.9 eV, and a highly damped peak at 8.4 eV. In addition in the UPS spectrum at x = 0.20, a slight blurring of the peaks at –6.4 and –5.4 eV occurs, and at the same time new peaks around –6.0 and –4.3 eV can be recognized. For the further increase of x, features of the UPS and IPES spectra reach those of g-$GeSe_2$. The UPS spectrum for g-$GeSe_2$ is in good agreement with previous data [17,18,19], and the IPES spectrum coincides well with our previous measurement [38].

5. Discussion

As mentioned before, it can be seen in Fig. 7(b) that a decrease of the Ge concentration x leads to a rapid decrease of the prepeak intensity in $S(Q)$, and its position considerable shifts to higher Q values. Fig. 11 shows the Q position of the prepeak, Q_p, and the intensity, $S(Q_p)$, as a function of x. Since the $S(Q)$ at x = 0.167 shows no longer a peak but a shoulder in the range of interest, a two-Gaussian fit was applied to obtain the Q_p and $S(Q_p)$. With decreasing x from x = 0.25 to 0.195, Q_p increases linearly. With the further decrease of x, Q_p increases much more rapidly (or shows a jump) between x = 0.195 and 0.185. At the same time, there is a noticable decrease of $S(Q_p)$ in this concentration range. For the further discussion of the prepeak or the IRO in this concentration range, it is essential to clarify the origin of the prepeak.

It can be seen at a glance from Figs. 8 and 9 that the height of the prepeak is much larger in $\Delta_{Ge}S(Q)$ than in $S(Q)$, whereas there is no characteristic feature seen in $\Delta_{Se}S(Q)$. As already pointed out in Sec III (see Fig. 2), the Ge-related W_{ij}s in $\Delta_{Ge}S(Q)$ are much larger than those in $S(Q)$, while W_{GeGe} in $\Delta_{Se}S(Q)$ is negligibly small. Thus it appears highly plausible to speculate that the prepeak originates from the Ge-Ge correlation in g-Ge_xSe_{1-x} in the concentration range near x = 0.20.

The same conclusion was recently reached by Petri *et al.* [39] for *g*-$GeSe_2$ from an analysis of neutron scattering experiments with isotope enriched samples. They observed a prepeak in the experimentally determined $S_{GeGe}(Q)$, which has almost the same height as of the first peak. On the other hand, almost no characteristic features were visible in $S_{GeSe}(Q)$ and $S_{SeSe}(Q)$ at the prepeak position. In addition, they observed a large minimum in $S_{GeSe}(Q)$ with negative sign at the first peak position in $S(Q)$.

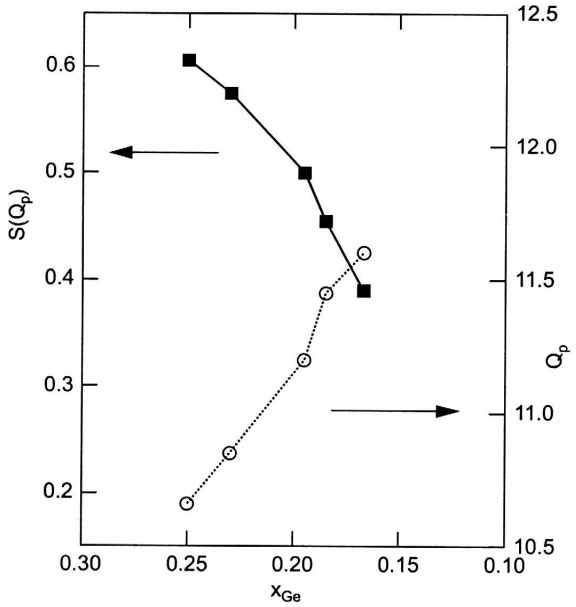

Fig. 11. The Q position of the prepeak, Q_p, and the intensity, $S(Q_p)$, as a function of the Ge concentration x.

For comparison, we calculated "*modeled*" spectra from the $S_{ij}(Q)$ data of Petri *et al.* [39] employing the W_{ij}s for *g*-$Ge_{0.195}Se_{0.805}$ and $Ge_{0.23}Se_{0.77}$. The dotted lines in Figs. 8 and 9 indicate the calculated spectra for *g*-$Ge_{0.195}Se_{0.805}$ and $Ge_{0.23}Se_{0.77}$, respectively. Surprisingly, the obtained spectra show features similar to our experimental $\Delta_i S(Q)$ and $S(Q)$ data. However, quantitatively there are large deviations from our experimental data in the Q ranges of the prepeak and the first peak. The height of the prepeak in each of our $\Delta_{Ge}S(Q)$ spectrum is much larger than that in the "*model*" spectrum (see dotted line). The same is also true for $S(Q)$. This is consistent with the speculation that the prepeak in $S_{GeGe}(Q)$ in this concentration region is much larger in height than that for $GeSe_2$.

For obtaining the local structural information (not only for confirming the above speculation) requested in this concentration range, it is, needless to say, crucial to directly obtain $S_{ij}(Q)$s from our AXS data. As seen in Figs 8 and 9, however, the obtained $\Delta_i S(Q)$s slightly lean to the left, although the $S(Q)$ data do not. Such slight slopes unfortunately produce a considerable error in $S_{ij}(Q)$s. This trend was also found in the previous AXS results by Armand *et al.* [15]. It prevents us from reaching the final goal of structural studies using the AXS technique. It can be pointed out that *f'* and/or *f"* seem to have small Q-dependencies.

For this reason, the analysis of the prepeak was performed under a very rough assumption that near the prepeak position the Se related $S_{ij}(Q)$s, *i.e.*, $S_{GeSe}(Q)$ and $S_{SeSe}(Q)$, in our concentration range are identical to those of *g*-$GeSe_2$ obtained by Petri *et al.* [39], and that only $S_{GeGe}(Q)$ can vary with x. The analysis was carried out using the $S(Q)$ data at x = 0.185, 0.195, and 0.23. Fig. 12 shows the estimated $S_{GeGe}(Q)$s (solid lines) near the prepeak position along with that of *g*-$GeSe_2$ (dashed line) obtained by Petri *et al.* [39]. As mentioned above, the prepeaks at x = 0.23 and 0.195 (almost the same as each other) are more than twice larger in height than that at x = 0.333. One can also see a rapid decrease of the prepeak height at x = 0.185 by only 1% further decrease of x. Based on these structural results on the prepeak or the IRO around the stiffness threshold composition, a further discussion is given later in combination with the results of the electronic structures.

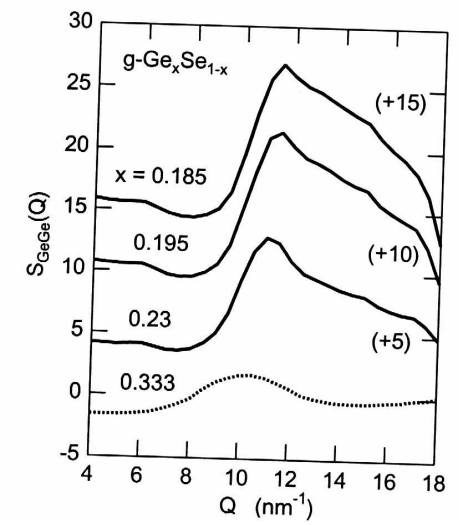

Fig. 12. Estimated $S_{GeGe}(Q)$s (solid lines) near the prepeak position along with that of g-$GeSe_2$ (dashed line) obtained by Petri *et al.* [39]. See text for details.

In Figs. 8 and 9, the heights of the first peaks in our $\Delta_{Se}S(Q)$ and $S(Q)$ spectra are much smaller than that of the calculated spectra (dotted lines), and the dips found in $\Delta_{Ge}S(Q)$ of the present work are much deeper. Since $S_{GeSe}(Q)$ dominates $\Delta_{Ge}S(Q)$, and the heights of the first peaks in $\Delta_{Se}S(Q)$ and $S(Q)$ are determined by compensating a large maximum in $S_{SeSe}(Q)$ for a large minimum in $S_{GeSe}(Q)$, one expects that $S_{GeSe}(Q)$s for x = 0.195 and 0.23 have much deeper minima at the first peak position than that for g-$GeSe_2$. Although $\Delta_i S(Q)$s could only be measured along limited Q ranges, it is instructive to perform Fourier transformations to obtain differential pair distribution functions $\Delta_i g(r)$ in order to examine the SRO around each constituent element. Fig. 13(a) and (b) show $\Delta_i g(r)$s of g-$Ge_{0.195}Se_{0.805}$ and $Ge_{0.23}Se_{0.77}$, respectively. Dashed and solid lines indicate $\Delta_i g(r)$s near the Ge and Se K edges, respectively. The first nearest neighbour distances around both Ge and Se are found to be 0.236 ± 0.002 nm in each concentration, which coincides with the previous scattering- [4,13,14] and XAFS [10-12] results within the experimental error.

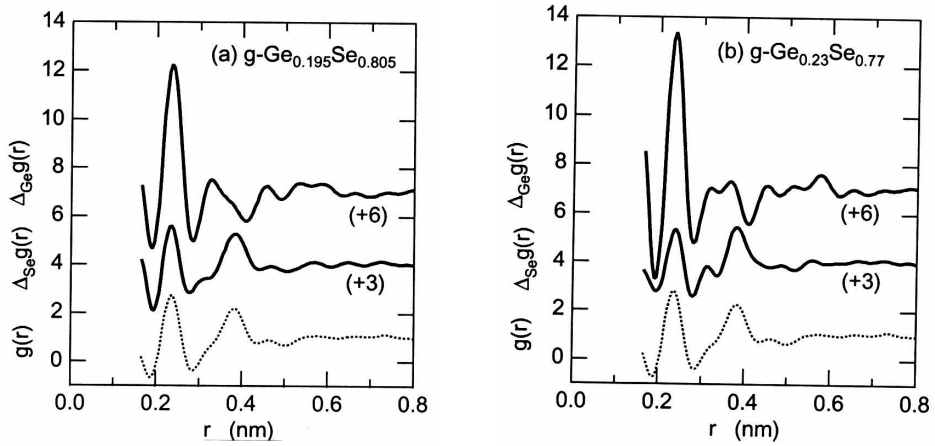

Fig. 13. $\Delta_i g(r)$s of (a) g-$Ge_{0.195}Se_{0.805}$ and (b) $Ge_{0.23}Se_{0.77}$ together with $g(r)$. Solid lines indicate $\Delta_i g(r)$s, and dashed lines $g(r)$s.

This result supports the model that the glasses in this concentration range have an SRO similar to the $GeSe_2$ crystal. As mentioned in the last section (see Fig. 10), the spectral shapes of both the valence-band UPS and the conduction-band IPES spectra remarkably change around the stiffness threshold composition x = 0.20 from g-$GeSe_2$-like to g-Se-like. They have characteristic peaks of their own in the spectra.

The character of peaks in the UPS spectra can be assigned using PES data with different energies of incident light, because the excitation cross-section is depend on the quantum number of the orbital angular momentum. The peak positions of the UPS spectra and their electronic states for *g*-$GeSe_2$ and *g*-Se are tabulated in Table 2. In *g*-$GeSe_2$, the top of the valence bands at –2.7 eV is formed by a lone-pair (LP) band of the Se 4p states. It is followed by two Ge 4p–Se 4p bonding (σ) states at –4.3 and –6.0 eV. When using a higher energy of incident light, one can also observe a Ge 4s–Se 4p bonding (σ) band around –9 eV and an Se 4s state around –14 eV [19]. In *g*-Se, the top of the valence bands is also formed by the Se LP state at –2.7 eV. Beneath it, two Se 4p bonding (σ) states are located at –5.4 and –6.4 eV. The Se 4s states are located around –12~–15 eV [20].

Table 2. Energy positions of peak structures in the UPS and IPES spectra on *g*-$GeSe_2$ and *g*- Se. These peaks are assigned to electronic states contributed predominantly.

	Energy (eV)	Electronic states
g-$GeSe_2$	–6.0 ⎫	
	⎬	σ [Ge sp^3 (4p-rich) – Se 4p]
	–5.4 ⎭	
	–2.7	lone pair [Se 4p]
	2.4	σ* [Ge sp^3 (4s-rich) – Se 4p]
	4.9	σ* [Ge sp^3 (4p-rich) – Se 4p]
	8.4	Ge 4d and/or 5s, Se 4d and/or 5s
g-Se	–6.4 ⎫	
	⎬	σ [Se 4p]
	-5.4 ⎭	
	–2.7	lone pair [Se 4p]
	3.1	σ* [Se 4p]
	7.4	Se 4d and/or 5s

The electronic state assignment can also be carried out for peaks in IPES spectra by comparing them with core-absorption spectra, which are affected by the selection rule of excitations from the core-level (s, p, or d) to the conduction band. The peak positions of the IPES spectra and their electronic character for *g*-$GeSe_2$ and *g*-Se are also tabulated in Table 2. In *g*-$GeSe_2$ [38], the bottom of conduction bands at 2.4 eV is formed by an antibonding (σ*) band with the Ge sp^3 (4s-rich) – Se 4p hybridized states. It is followed by an antibonding (σ*) band with the Ge sp^3 (4p-rich) – Se 4p hybridized states at 4.9 eV, and the 4d and /or 5s states of both Ge and Se at 8.4 eV. In *g*-Se [23], the bottom of the conduction bands at 3.1 eV is formed by an antibonding (σ*) band with the Se 4p states. It is followed by the Se 4d and /or 5s states at 7.4 eV.

Noteworthy questions are why the electronic structure of *g*-Ge_xSe_{1-x} does not vary gradually from *g*-$GeSe_2$-like to *g*-Se-like with *x*, but shows a sudden (transition-like) change around the stiffness threshold composition $x = 0.20$, and why the prepeak in $S_{GeGe}(Q)$ or the IRO of the Ge-Ge correlation enhances at this composition. In order to solve these questions, it seems worthwhile to recall an old idea by Feltz *et al.* [40]. They examined the concentration dependence of several physical properties of *g*-Ge_xSe_{1-x}, such as dielectric constant, molar volume, glass transition temperature, and thermal expansion coefficient. As a result, they came to the conclusion that $GeSe_4$ ($x = 0.20$) is a new non-crystalline compound which exists in the liquid or glassy state, and there, $Ge(Se_{1/2})_4$ units should be predominantly linked by Se-Se bridges.

Based on this concept, one can try to explain our experimental results. At $x = 0.33$, $Ge(Se_{1/2})_4$ tetrahedra are linked to each other by their edge- or corner-sharing, *i.e.*, the Ge-Ge correlation is always $(Se_{1/2})_3Ge–Se–Ge(Se_{1/2})_3$. With decreasing *x* from 0.33 to 0.20, successive structural changes occur from the direct connection at $x = 0.33$ to two-Se-linked tetrahedra at $x = 0.20$, *i.e.*, $(Se_{1/2})_3Ge–Se–Se–Ge(Se_{1/2})_3$ all over the material. The Ge-Ge correlation in *g*-$Ge_{0.20}Se_{0.80}$ still exists by forming these connections because the correlation-length of this new connection is well defined. The

correlation is even stronger than in *g*-$GeSe_2$ due to the relaxed formation of the connections. The gradual movements of the prepeak would be caused by these reconnections of the $Ge(Se_{1/2})_4$ tetrahedra. With further decrease of *x*, the tetrahedra become isolated and are connected by short chains, *i.e.*, $(Se_{1/2})_3Ge–Se–Se–Se–Ge(Se_{1/2})_3$ as the shortest case. Due to the flexible conformation of this connection, the Ge-Ge correlation length of this connection is no longer well defined, and the prepeak starts to disappear with *x*. It seems to be much more difficult to explain the concentration change of the electronic structure using this simple atomic structure model. This is because this requires the additional constraints that the electronic structure of the $(Se_{1/2})_3Ge–Se–Se–Ge(Se_{1/2})_3$ conformation at $x = 0.20$ should be very similar to that of $(Se_{1/2})_3Ge–Se–Ge(Se_{1/2})_3$ in *g*-$GeSe_2$, and that of $(Se_{1/2})_3Ge–Se–Se–Se–Ge(Se_{1/2})_3$ at $x < 0.20$ should be identical to that of Se chains. Molecular orbital band calculation would be useful to estimate the energy positions of the corresponding bonding-, lone-pair-, and antibonding states in the above small fragments. For this, however, precise structural determinations for several concentrations near the stiffness threshold composition, *i.e.*, the information of $S_{ij}(Q)$s, is essential. Further AXS investigations are now in progress.

6. Conclusion

Anomalous x-ray scattering experiments on glassy Ge_xSe_{1-x} were carried out at energies close to the Ge and Se K edges at both the onset and completion concentrations of the rigidity percolation threshold. The total structure factors $S(Q)$ show rapid changes in both the position and intensity of the prepeak around 10 nm^{-1}, while remain almost unchanged in the other Q ranges. The differential structure factors $\Delta_i S(Q)$ obtained have characteristic features of their own, which suggest that the prepeak originates from only the Ge-Ge concentration. The origin of the prepeak was discussed in the sight of the concentration dependence of the spectra and a comparison with the partial structure factors on glassy $GeSe_2$ obtained by Petri *et al.* [39].

Valence- and conduction-band electronic density of states were investigated on glassy Ge_xSe_{1-x} ($0 \le x \le 0.33$) by measuring ultraviolet photoemission and inverse-photoemission spectra. They exhibit a distinct change in their spectral features near $x = 0.20$.

These observations in both the atomic and electronic structures are consistent with an occurrence of percolation threshold in non-crystalline covalent network systems predicted by Phillips and Thorpe. The threshold is characterized by the percolation of a specific $Ge(Se_{1/2})_4$ molecular unit spread over the network.

Acknowledgements

The AXS work was performed in collaboration with Dr. D. Raoux and Dr. J.-F. Bérar of CNRS/Grenoble, Prof. K. Murase and Dr. Y. Wang of Osaka University, and Dr. W.-C. Pilgrim and Dr. J. Greif of Philipps Universität Marburg. It was supported by the Deutsche Forschungs Gemeinschaft (DFG) and the Bundesministeriums für Bildung, Wissenschaft, Forschung und Technilogie (Bmbf). The PES and IPES measurements were performed in collaboration with Prof. M. Tanuguchi and his coworkers in Hiroshima University, and Prof. K. Murase of Osaka University. They were partially supported by the Grant-in-Aid for Scientific Research from the Ministry of Education, Science, and Culture, Japan.

References

[1] W. H. Zachariasen, J. Am. Chem. Soc. **54**, 3841 (1932).
[2] R. W. Fawcett, C. N. J. Wagner, G. S. Cargill III, J. Non-Cryst. Solids **8-10**, 369 (1972).
[3] O. Uemura, Y. Sagara, T. Satow, Phys. Stat. Sol. (a) **26**, 99 (1974).
[4] T. Satow, O. Uemura, Y. Sagara, J. Jpn. Inst. Met. **37**, 1348 (1973) (in Japanese).
[5] P. Tronc, M. Bensoussan, A. Brenac, C. Sebenne, Phys. Rev. B **8**, 5947 (1973).
[6] J. C. Phillips, J. Non-Cryst. Solids **34**, 153 (1979).
[7] M. F. Thorpe, J. Non-Cryst. Solids **57**, 355 (1983).
[8] W. A. Katamigahara, R. L. Cappelletti, P. Boolchand, B. Halfpap, F. Gompf, D. A. Neumann, H. Mutka, Phys. Rev. B **44**, 94 (1991).

[9] X. Feng, W. J. Bresser, P. Boolchand, Phys. Rev. Lett. **78**, 4422 (1997).
[10] C. Peyroutou, S. Peytavin, M. Ribes, J. Solid State Chem. **82**, 78 (1989).
[11] W. Zhou, M. Paesler, D. E. Sayers, Phys. Rev. B **43**, 2315 (1991).
[12] E. Gulbrandsen, H. B. Johnsen, M. Endregaard, T. Grande, S. Stølen, J. Solid State Chem. **145**, 253 (1999).
[13] J. C. Malaurent, J. Dixmier, J. Non-Cryst. Solids **35&36**, 1227 (1980).
[14] N. R. Rao, P. S. R. Krishna, S. Basu, B. A. Dasannacharya, K. S. Sangunni, E. S. R. Gopal, J. Non-Cryst. Solids **240**, 221 (1998).
[15] P. Armand, A. Ibanez, Q. Ma, D. Raoux, E. Philippot, J. Non-Cryst. Solids **167**, 37 (1993).
[16] S. Hosokawa, Y.Wang, J.-F. Bérar, J. Greif, W.-C. Pilgrim, D. Raoux, K. Murase, Phys. Chem. Chem. Phys, to be submitted.
[17] S. Hino, T. Takahashi, Y. Harada, Solid State Commun. **35**, 379 (1980).
[18] T. Ueno, A. Odajima, Jpn. J. Appl. Phys. **21**, 1382 (1982).
[19] K. Inoue, T. Katayama, K. Kawamoto, and K. Murase, Phys. Rev. B **35**, 7496 (1987).
[20] N. J. Shevchik, M. Cardona, J. Tejeda, Phys Rev. B **8**, 2833 (1973).
[21] D. E. Aspnes, J. C. Philipps, K. L. Tai, P. M. Bridenbaugh, Phys. Rev. B **23**, 816 (1981).
[22] J. Stuke, J. Non-Cryst. Solids **4**, 1 (1970).
[23] S. Hosokawa, Y. Hari, K. Nishihara, M. Tamura, M. Taniguchi, J. Non-Cryst. Solids **164-166**, 1199 (1993).
[24] S. Hosokawa, H. Sato, K. Nishihara, Y. Hari, M. Taniguchi, J. Non-Cryst. Solids **250-252**, 415 (1999).
[25] J. Bordas, J. B. West, Philos. Mag. **34**, 501 (1976).
[26] E. Belin, C. C. Sememaud, S. Guita, Philos. Mag. B **63**, 1159 (1991).
[27] S. Hosokawa, T. Kouchi, I. Ono, M. Taniguchi, Y. Takata, N. Kosugi, J. Phys.: Condens. Matter **8**, 1607 (1996).
[28] M. Taniguchi, T. Kouchi, I. Ono, S. Hosokawa, M. Nakatake, H. Namatame, K. Murase, J. Electron Spectrosc. Relat. Phenom. **78**, 507 (1996).
[29] S. Sasaki, KEK Report 1989 (Nat. Lab. High Energy Phys., Tsukuba, Japan), p. 1.
[30] T. Kawamura, T. Fukamachi, Jpn. J. Appl. Phys. Suppl. **17-2**, 228 (1978); T. Fukamachi, S. Hosoya, T. Kawamura, M. Okunuki, Acta Cryst. A **35**, 104 (1979).
[31] P. H. Fuoss, W. K. Warburton, A. Bienenstock, J. Non-Cryst. Solids **35&36**, 1233 (1980).
[32] U. Bonse, I. Hartmann-Lotsch, H. Lotsch, K. Olthoff-Mienter, Z. Phys. B **47**, 297 (1982).
[33] C. H. MacGillavry, G. D. Rieck (ed.), International Tables for X-ray Crystallographie, 2nd ed., (Kynoch, Birmingham, 1968), Vol. III.
[34] K. Yokoyama, K. Nishihara, K. Mimura, Y. Hari, M. Taniguchi, Y. Ueda, M. Fujisawa, Rev. Sci. Instrum. **64**, 87 (1993).
[35] Y. Ueda, K. Nishihara, K. Mimura, Y. Hari, M. Taniguchi, M. Fujisawa, Nucl. Instrum. Methods A **330**, 140 (1993).
[36] J. Krogh-Moe, Acta Cryst. **9**, 951 (1956).
[37] N. Norman, Acta Cryst. **10**, 370 (1957).
[38] S. Hosokawa, K. Nishihara, Y. Hari, M. Taniguchi, O. Matsuda, K. Murase, Phys. Rev. B **47**, 15509 (1993).
[39] I. Petri, P. S. Salmon, H. E. Fischer, Phys. Rev. Lett. **84**, 2413 (2000).
[40] A. Feltz, H. Aust, A. Blayer, J. Non-Cryst. Solids **55**, 179 (1983).